Spin Density and Structure of Aquabis(2,2'-bipyridine)di-μ-hydroxo-sulphatodicopper(II) Tetrahydrate at 4.2 K †

Brian N. Figgis
School of Chemistry, The University of Western Australia, Nedlands, Western Australia 6009, Australia
Ronald Mason, Andrew R. P. Smith, and Joseph N. Varghese
School of Molecular Sciences, The University of Sussex, Brighton, Sussex BN1 9QJ
Geoffrey A. Williams*
Australian Radiation Laboratory, Lower Plenty Road, Yallambie, Victoria 3085, Australia

The spin density distribution in the metal–ligand framework of the title compound has been determined from two-dimensional polarised neutron diffraction data. A qualitative picture of the superexchange pathway between copper atoms in the dimeric molecule emerges, and the importance of spin polarisation effects is indicated by the presence of significant regions of negative spin density on the sides of the bridging oxygen atoms away from the copper atoms. The important role played by the spin polarisation phenomenon in the exchange process indicates the need for a full *unconstrained* Hartree–Fock calculation in any theoretical treatment of the CuO_2Cu system. As a necessary corollary to the spin density study, the molecular structure of $[(H_2O)(bipy)Cu(OH)_2Cu(bipy)(OSO_3)]\cdot 4H_2O$ (bipy = 2,2'-bipyridine) has been determined at 4.2 K by single-crystal neutron diffraction methods from limited three-dimensional intensity data. Crystals are monoclinic, space group $P2_1/c$, with a = 9.658(12), b = 34.29(3), c = 7.626(10) Å, β = 103.3(1)°, and Z = 4.

A series of binuclear copper complexes,[1] formulated as $[LCu(OH)_2CuL]X\cdot nH_2O$ where L = 1,10-phenanthroline or 2,2'-bipyridine (bipy) and X = a variety of mono- and bivalent anions, has been studied by single-crystal *X*-ray diffraction [2,3] and by magnetic susceptibility measurements over the temperature range 4.2—298 K.[2,4–6] For all the compounds studied, the room-temperature magnetic moments per copper atom were found to be well above the spin-only value and of *ca.* 2.0 B.M.[1]

The magnetic susceptibility of the title compound, $[(H_2O)(bipy)Cu(OH)_2Cu(bipy)(OSO_3)]\cdot 4H_2O$, was observed to obey the Curie–Weiss law with θ = −11 K over the temperature range 35—298 K.[2,5] Below 35 K, the magnetic susceptibility of the complex departs from the Curie–Weiss law,[5] and this behaviour is interpreted in terms of exchange-coupled copper atoms, with a positive value (49 cm^{-1}) of the singlet–triplet splitting or exchange parameter, $2J$. A positive value of $2J$ indicates that the complex has a triplet ground state, with the singlet level of the dimer being somewhat higher in energy. It has been pointed out [2,3] that this type of ferromagnetic coupling between the copper atoms is unusual, because antiferromagnetic interactions generally occur in binuclear complexes containing oxygen-bridged copper atoms.

Possible mechanisms for the exchange interaction between the copper atoms in $[(H_2O)(bipy)Cu(OH)_2Cu(bipy)(OSO_3)]$ have been discussed in terms of either direct overlap of metal orbitals, or a metal–oxygen–metal pathway.[6,7] The system has been studied theoretically by use of extended Huckel molecular orbital calculations.[7] It has also been shown that, for a number of related compounds,[8] a correlation exists between the singlet–triplet splitting, $2J$, and the Cu–O–Cu bridge angle.

A more complete understanding of the exchange processes involved in these dimeric copper complexes obviously entails a characterization of the spatial distribution of the unpaired electron density around the copper atoms. The spin density distribution, and hence the magnitude of the coupling, is expected to be very much a function of the copper atom environments. We have in hand a program to study the spin density distributions in transition-metal compounds by use of the technique of polarised neutron diffraction (p.n.d.).[9] Analyses already undertaken , on the CrF_6^{3-} ion in $K_2Na[CrF_6]$,[10–12] on the $CoCl_4^{2-}$ ion in Cs_3CoCl_5,[13,14] and on the cobalt [15] and manganese [16] complexes of the phthalocyanine ligand, have successfully defined the spatial distribution of spin density on the metal and ligand atoms with worthwhile accuracy.

We report here the molecular structure of $[(H_2O)(bipy)Cu(OH)_2Cu(bipy)(OSO_3)]\cdot 4H_2O$ at 4.2 K determined by single crystal neutron diffraction techniques, together with a p.n.d. determination of the spin density distribution at 4.2 K in the complex. A preliminary report of this work has already been published.[17]

Experimental

The compound $[(H_2O)(bipy)Cu(OH)_2Cu(bipy)(OSO_3)]\cdot 4H_2O$ was prepared by a method essentially analogous to that given in ref. 4. Large blue single crystals suitable for neutron diffraction studies were obtained by slow evaporation of an aqueous acetone solution of the compound.

Molecular Structure Determination.—Crystal data for both the present study, and the *X*-ray diffraction study at 295 K,[2,3] are presented in Table 1. Neutron diffraction intensity data were obtained at 4.2 K and λ = 1.175 Å on the D15 normal-beam diffractometer with motorised lifting counter, located at a thermal neutron inclined beam of the Institut Laue-Langevin high-flux reactor. Two intensity data sets were obtained from two different crystals. The first (crystal 1), of dimensions 4.0 × 1.4 × 1.0 mm, was mounted with its *a* axis offset by *ca.* 5° from the ω—2θ diffractometer axis in order to minimise multiple diffraction effects. The second (crystal 2), of dimensions 4.0 × 1.3 × 1.4 mm, was mounted with its *c* axis similarly offset from the ω—2θ diffractometer axis. The space group was verified to be $P2_1/c$ by confirming the systematic absences $0k0$ for k odd, and $h0l$ for l odd, on the diffractometer. Unit-cell parameters, together with their estimated standard deviations (e.s.d.s), were derived by a least-squares

† *Supplementary data available* (No. SUP 23495, 22 pp.): thermal parameters, magnetic structure factors, nuclear structure factors (both crystals 1 and 2). See Notices to Authors No. 7, *J. Chem. Soc., Dalton Trans.*, 1981, Index issue.

Non-S.I. unit employed: B.M. = 0.927 × 10^{-23} A m^2.

analysis of the setting angles determined for 10 angularly well separated reflections for each crystal, and the final parameters and e.s.d.s given in Table 1 are average values.

Throughout the data collection, the temperature was monitored and remained steady at 4.2 ± 0.1 K. Intensities were measured *via* an ω—θ scan which was found to be appropriate for the mosaic spreads of the crystals. There was no significant variation in the intensity of a standard reflection during data collection on each crystal. We could not hope to obtain a complete three-dimensional intensity data set within any reasonable $(\sin\theta)/\lambda$ limit, due to the large unit cell (and hence large number of possible Bragg reflections) and the finite measuring time available (20 d). The cryostat design on the D15 diffractometer imposed a limit on the height of the lifting detector above the equatorial plane, and only *hkl* data with $h \leqslant 3$ were obtained from crystal 1. From crystal 2, only data with $l = 0$ were obtained. A problem affecting the quality of the measured intensity data was the lack of resolution along the *b*-axis direction, due to the large *b*-axis length. This meant that in certain cases two neighbouring Bragg peaks could not be resolved. All reflections where the measured Bragg intensities were obviously in error due to this resolution problem were discarded from the final data set used in the structure refinement. In the case of crystal 2, the mosaic spread was considerably larger than for crystal 1, and the resolution problem was therefore greater. Upon removal of crystal 2 from the liquid helium cryostat it was found to have fractured, presumably due to thermal shock, thereby explaining the observed behaviour.

All intensity data that could be obtained within the limit $(\sin\theta)/\lambda \leqslant 0.75$ Å^{-1} were collected, and in many cases two or more equivalent reflections were measured. For the *hk*0 data from crystal 2 in particular, as many equivalent reflections as possible were measured, and lack of agreement was taken to indicate a resolution problem. Integrated intensities were obtained by use of a profile-analysis program, COLL5,[18] and geometrical corrections were applied. Absorption corrections were not considered necessary due to the small linear absorption coefficient (Table 1). The intensities of equivalent reflections were averaged. A final data set containing 1 483 unique reflections from crystal 1, and 385 unique *hk*0 reflections from crystal 2, was used in the structure refinement.

The structure was refined by use of the least-squares program CRYLSQ[19] in the full-matrix mode. The function minimised was $\Sigma w(\Delta F)^2$ where *w* is the weight, based on counting statistics and a comparison of equivalent reflections, assigned to the $|F_o|$ values, and $\Delta F = |F_o| - |F_c|$. Starting parameters were obtained from the *X*-ray analysis at 295 K,[3] with the exception of H atoms which were initially placed in

Table 1. Crystal data for $[(H_2O)(bipy)Cu(OH)_2Cu(bipy)(OSO_3)]\cdot 4H_2O$ [a]

	295 K [b]	4.2 K
a/Å	9.683(3)	9.658(12)
b/Å	34.52(1)	34.29(3)
c/Å	7.822(3)	7.626(10)
β/°	103.50(2)	103.3(1)
U/Å^3	2 542.3	2 457.8
D_c/Mg m^{-3}	1.723	1.782
λ/Å	1.5418	1.175
μ/mm^{-1}	3.43	0.185 [c]

[a] $C_{20}H_{28}Cu_2N_4O_{11}S$, $M = 659.6$, space group $P2_1/c$, $Z = 4$. [b] See refs. 2 and 3. [c] Includes an estimate of the incoherent scattering contribution.

Table 2. Final atomic positional co-ordinates for $[(H_2O)(bipy)Cu(OH)_2Cu(bipy)(OSO_3)]\cdot 4H_2O$

Atom	*X*/*a*	*Y*/*b*	*Z*/*c*	Atom	*X*/*a*	*Y*/*b*	*Z*/*c*
Cu(1)	0.071 8(10)	0.089 5(1)	0.195 9(6)	C(24)	0.551 0(12)	0.221 2(1)	0.418 6(7)
Cu(2)	0.178 6(10)	0.164 9(1)	0.116 7(6)	C(34)	0.516 3(12)	0.260 6(1)	0.382 3(7)
O(1)	0.008 2(13)	0.132 0(1)	0.023 4(8)	C(44)	0.389 6(12)	0.270 8(1)	0.269 3(6)
O(2)	0.251 7(15)	0.120 5(1)	0.272 4(8)	C(54)	0.297 2(11)	0.241 3(1)	0.198 5(7)
O(3)	0.296 0(13)	0.148 6(1)	−0.074 6(7)	S	0.289 2(27)	0.118 3(3)	−0.214 1(17)
O(4)	0.387 3(14)	0.084 4(1)	−0.152 9(7)	H(1)	0.045 8(25)	0.121 8(2)	−0.093 7(15)
O(5)	0.122 9(13)	0.105 3(1)	−0.262 0(8)	H(2)	0.267 6(28)	0.126 1(3)	0.399 6(17)
O(6)	0.333 8(13)	0.134 9(1)	−0.374 4(8)	H(11)	−0.212 7(26)	0.094 5(3)	−0.065 0(16)
O(7)	−0.023 6(17)	0.116 0(2)	0.407 8(15)	H(21)	−0.425 1(29)	0.049 0(3)	−0.167 8(17)
O(8)	0.705 2(14)	0.127 4(2)	0.381 8(9)	H(31)	−0.403 6(30)	−0.021 1(3)	−0.065 4(16)
O(9)	0.488 0(13)	0.084 0(1)	0.209 5(9)	H(41)	−0.158 0(25)	−0.040 9(3)	0.153 8(14)
O(10)	−0.254 3(14)	0.163 2(1)	0.055 8(9)	H(12)	0.333 3(26)	0.063 2(3)	0.479 4(14)
O(11)	0.612 4(15)	0.144 4(2)	−0.304 6(10)	H(22)	0.439 4(31)	−0.001 6(3)	0.630 2(17)
N(1)	−0.089 8(9)	0.053 6(1)	0.092 2(5)	H(32)	0.231 1(28)	−0.058 9(3)	0.554 3(15)
N(2)	0.140 6(9)	0.040 0(1)	0.326 8(5)	H(42)	0.036 2(25)	−0.052 0(3)	0.327 8(14)
N(3)	0.082 0(8)	0.214 9(1)	0.007 5(5)	H(13)	−0.096 0(28)	0.190 6(3)	−0.162 4(14)
N(4)	0.324 7(7)	0.203 1(1)	0.236 6(4)	H(23)	−0.203 9(23)	0.254 3(3)	−0.272 9(15)
C(11)	−0.217 0(12)	0.064 2(1)	−0.020 9(7)	H(33)	−0.059 4(26)	0.316 1(2)	−0.150 4(14)
C(21)	−0.324 6(12)	0.038 4(1)	−0.077 3(7)	H(43)	0.182 1(22)	0.310 8(3)	0.069 7(14)
C(31)	−0.298 2(16)	−0.000 2(1)	−0.017 0(7)	H(14)	0.473 5(28)	0.162 2(3)	0.369 2(14)
C(41)	−0.183 8(12)	−0.011 2(1)	0.102 6(7)	H(24)	0.642 4(29)	0.211 8(3)	0.512 7(16)
C(51)	−0.080 4(12)	0.016 8(1)	0.154 7(6)	H(34)	0.618 4(28)	0.283 9(3)	0.444 7(16)
C(12)	0.269 2(11)	0.036 7(1)	0.450 3(7)	H(44)	0.348 2(29)	0.301 2(3)	0.237 7(15)
C(22)	0.306 9(16)	0.001 3(1)	0.530 6(6)	H(71)	0.025 5(32)	0.113 0(3)	0.522 4(16)
C(32)	0.228 6(13)	−0.031 0(1)	0.488 1(7)	H(72)	−0.113 5(32)	0.117 7(4)	0.405 0(29)
C(42)	0.098 6(13)	−0.027 0(1)	0.364 0(6)	H(81)	0.625 4(30)	0.110 4(3)	0.315 4(17)
C(52)	0.063 7(13)	0.009 0(1)	0.286 7(6)	H(82)	0.669 9(28)	0.133 7(3)	0.493 6(17)
C(13)	−0.048 3(11)	0.217 7(1)	−0.115 2(7)	H(91)	0.472 9(29)	0.084 9(3)	0.083 1(16)
C(23)	−0.097 8(10)	0.253 7(1)	−0.171 5(7)	H(92)	0.380 1(30)	0.096 9(3)	0.238 1(18)
C(33)	−0.020 3(13)	0.287 8(1)	−0.102 8(7)	H(101)	−0.143 1(31)	0.151 7(3)	0.062 0(20)
C(43)	0.117 8(12)	0.284 6(1)	0.016 7(7)	H(102)	−0.275 1(27)	0.153 4(3)	0.155 4(16)
C(53)	0.166 9(8)	0.248 0(1)	0.070 3(7)	H(111)	0.533 4(30)	0.139 7(3)	−0.324 1(20)
C(14)	0.444 9(11)	0.193 5(1)	0.344 8(7)	H(112)	0.643 7(30)	0.151 7(3)	−0.179 8(16)

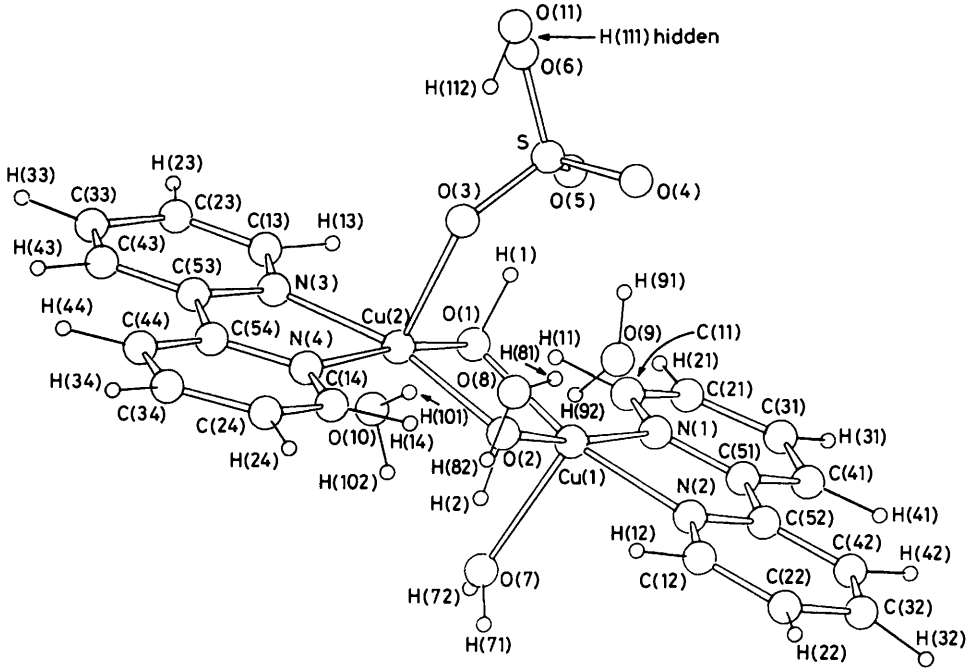

Figure 1. The geometry and atom numbering of $[(H_2O)(bipy)Cu(OH)_2Cu(bipy)(OSO_3)]\cdot 4H_2O$. Spheres, representing atoms, are on an arbitrary scale. Hydrogen atoms are represented as small spheres, and are numbered according to the atom to which they are attached

idealised positions. All atoms were assigned variable isotropic thermal parameters. The refinements of the thermal and positional parameters were performed in alternate, successive cycles.

For all 1868 reflections, the refinement cycles (266 variables including positional, thermal, and two scale parameters) converged with R ($=\Sigma|\Delta F|/\Sigma|F_o|$) 0.124 and R' { $= [\Sigma w(\Delta F)^2/\Sigma w|F_o|^2]^{\frac{1}{2}}$} 0.066. Because of the uncertainty introduced into the data of crystal 2 by the fracturing of the crystal, it was decided to remove these data from the final refinement cycles. The x-positional parameters were held invariant with values determined from the refinement using all data, because the remaining data have poor resolution in the a-axis direction. The 1 483 crystal 1 data were used to refine the y and z positional parameters together with isotropic thermal parameters which were refined separately as before. These refinement cycles (199 variables) converged with R 0.107 and R' 0.051. The maximum parameter shift-to-error ratio at convergence was 0.12 : 1. The neutron scattering lengths were taken from ref. 20 for all atoms. Final atomic positional parameters are listed in Table 2.

Obtaining Magnetic Structure Factors.—Polarised neutron diffraction 'flipping ratios' [21] were obtained at 4.2 K on the D3 normal-beam diffractometer located at a thermal neutron beam of the Institut Laue-Langevin high-flux reactor. The maximum flux available at the sample was *ca.* 3×10^{10} neutrons m^{-2} s^{-1}. Data were obtained over a total period of 28 d from two different crystals. Each crystal was aligned with its c axis coincident with the ω—2θ diffractometer axis, and a magnetic field of 4.6 T was applied along this direction. Only $hk0$ Bragg reflections were measured, as the copper and bridging oxygen atoms of major interest were well separated in a projection onto the ab crystal plane. In general, *ca.* 30 min were spent on each measurement of a flipping ratio. For each Bragg reflection, the measurement was repeated several times to improve counting statistics and, where possible, the accessible symmetry equivalents were also measured. Only those reflections with moderate to large *nuclear* intensities were measured, as the weaker reflections required much greater measuring times for worthwhile statistical accuracy.

From the first crystal of dimensions 3.0 × 2.7 × 1.5 mm, flipping ratios were measured at $\lambda = 0.986$ Å within the limit $(\sin\theta)/\lambda \leq 0.7$ Å^{-1}. Corrections for imperfect beam polarisation and for flipping efficiency were made, and the flipping ratios were converted to γ values by use of previously detailed formulae,[21] where $\gamma(hkl) = F_M(hkl)/F_N(hkl)$ is the ratio of magnetic [$F_M(hkl)$] and nuclear [$F_N(hkl)$] structure factors. For equivalent Bragg reflections, $\gamma(hkl)$ values were combined, yielding 150 unique, non-equivalent observations. The standard deviation in each γ value, $\sigma(\gamma)$, was determined from counting statistics. Phased F_M values, on absolute scale (B.M./unit cell), together with standard deviations $\sigma(F_M)$, were obtained from the γ and $\sigma(\gamma)$ values by use of F_N values *calculated* from the nuclear structure refinement at 4.2 K.

From the second crystal of dimensions 4.0 × 1.3 × 1.4 mm, flipping ratios of the same 150 unique reflections were re-measured at $\lambda = 0.893$ Å in order to increase the statistical accuracy of the data. These flipping ratios were converted to F_M values as before. The two F_M data sets obtained from the different crystals, and at different wavelengths, were in excellent agreement and were combined. This combined set of 150 unique $F_M(hkl)$ values was used in the subsequent modelling procedure described below.

For three reflections with strong nuclear intensities, ω—2θ scans through the Bragg peaks were performed to determine any systematic changes in flipping ratios with intensity. No systematic effects were observed and this, together with the wavelength invariance of the data, suggests that extinction effects in the data are insignificant.

Results and Discussion

The Molecular Structure.—The molecular geometry and atom numbering of the $[(H_2O)(bipy)Cu(OH)_2Cu(bipy)(OSO_3)]$ molecule at 4.2 K are shown in Figure 1. Interatomic bond

Table 3. Interatomic bond distances (Å) involving non-hydrogen atoms in $[(H_2O)(bipy)Cu(OH)_2Cu(bipy)(OSO_3)]$

	295 K (*X*-ray)	4.2 K (neutron) *		295 K (*X*-ray)	4.2 K (neutron) *
Cu(1)–O(1)	1.948(5)	1.96(1)	C(13)–C(23)	1.42(1)	1.36(1)
Cu(1)–O(2)	1.917(5)	2.00(1)	C(14)–C(24)	1.40(1)	1.42(1)
Cu(2)–O(1)	1.947(5)	1.99(1)	C(21)–C(31)	1.42(1)	1.40(1)
Cu(2)–O(2)	1.942(5)	1.96(1)	C(22)–C(32)	1.37(1)	1.34(1)
Cu(1)–N(1)	1.997(6)	2.00(1)	C(23)–C(33)	1.36(1)	1.42(1)
Cu(1)–N(2)	1.999(6)	2.00(1)	C(24)–C(34)	1.41(1)	1.40(1)
Cu(2)–N(3)	2.021(6)	2.04(1)	C(31)–C(41)	1.40(1)	1.32(1)
Cu(2)–N(4)	1.988(6)	1.99(1)	C(32)–C(42)	1.39(1)	1.39(1)
Cu(1)–O(7)	2.244(5)	2.23(1)	C(33)–C(43)	1.42(1)	1.44(1)
Cu(2)–O(3)	2.207(5)	2.12(1)	C(34)–C(44)	1.38(1)	1.37(1)
S–O(3)	1.461(6)	1.48(1)	C(41)–C(51)	1.38(1)	1.38(1)
S–O(4)	1.454(6)	1.50(2)	C(42)–C(52)	1.41(1)	1.38(1)
S–O(5)	1.469(6)	1.62(3)	C(43)–C(53)	1.39(1)	1.37(1)
S–O(6)	1.461(6)	1.50(2)	C(44)–C(54)	1.38(1)	1.38(1)
N(1)–C(11)	1.35(1)	1.38(1)	N(1)–C(51)	1.35(1)	1.35(1)
N(2)–C(12)	1.33(1)	1.38(1)	N(2)–C(52)	1.36(1)	1.29(1)
N(3)–C(13)	1.33(1)	1.39(1)	N(3)–C(53)	1.35(1)	1.42(1)
N(4)–C(14)	1.35(1)	1.30(1)	N(4)–C(54)	1.35(1)	1.35(1)
C(11)–C(21)	1.38(1)	1.36(1)	C(51)–C(52)	1.48(1)	1.54(1)
C(12)–C(22)	1.41(1)	1.37(1)	C(53)–C(54)	1.47(1)	1.42(1)

* Values in parentheses are the usual e.s.d.s from the least-squares fitting process, and may underestimate the actual inaccuracies in the 4.2 K neutron structural parameters.

Table 4. Interatomic bond distances (Å) involving hydrogen atoms in $[(H_2O)(bipy)Cu(OH)_2Cu(bipy)(OSO_3)]\cdot 4H_2O$ at 4.2 K

H(1)–O(1)	1.09(2)	H(14)–C(14)	1.11(1)
H(2)–O(2)	0.97(1)	H(24)–C(24)	1.05(2)
H(11)–C(11)	1.10(1)	H(34)–C(34)	1.27(2)
H(21)–C(21)	1.11(2)	H(44)–C(44)	1.12(1)
H(31)–C(31)	1.23(3)	H(71)–O(7)	0.90(2)
H(41)–C(41)	1.10(1)	H(72)–O(7)	0.87(3)
H(12)–C(12)	1.09(2)	H(81)–O(8)	1.01(2)
H(22)–C(22)	1.33(3)	H(82)–O(8)	1.01(2)
H(32)–C(32)	1.08(1)	H(91)–O(9)	0.94(1)
H(42)–C(42)	1.05(2)	H(92)–O(9)	1.20(3)
H(13)–C(13)	1.06(1)	H(101)–O(10)	1.13(3)
H(23)–C(23)	1.13(2)	H(102)–O(10)	0.90(2)
H(33)–C(33)	1.07(1)	H(111)–O(11)	0.76(3)
H(43)–C(43)	1.11(1)	H(112)–O(11)	0.96(1)

distances and selected angles, with estimated standard deviations derived from the refinement, are given in Tables 3—5. Selected intramolecular and intermolecular contact distances are given in Table 6.

The structure is essentially the same as that reported from the room-temperature *X*-ray analysis.[3] Because of the limitations in both the quality and extent of the intensity data at 4.2 K, as discussed above, no detailed comparison of the 4.2 K neutron and room-temperature *X*-ray structures is warranted. Bond distances in the two cases are presented side by side in Table 3.

The feature of the structure which has been defined with improved accuracy from the neutron analysis is the network of hydrogen bonds (Table 7). Hydrogen atom positions, tentatively assigned from a final difference synthesis in the *X*-ray analysis, have been confirmed with one exception in the present study. The position of one of the hydrogen atoms bound to O(10) [H(101) in the present study] differs from that given with fractional co-ordinates −0.15, 0.17, 0.17 in the *X*-ray analysis.[3] This means that this hydrogen atom is involved in a hydrogen bond with the bridging oxygen atom O(1) (Table 7), rather than with $O(11^I)$ as suggested previously [3] [from the neutron structure we have $O(11^I)\cdots H(101)$ 3.23(2) Å and angle $O(10)–H(101)\cdots O(11^I)$ 60°]. The starting position of H(101) in the present refinement of the neutron data was

Table 5. Selected bond angles (°) in $[(H_2O)(bipy)Cu(OH)_2Cu(bipy)(OSO_3)]\cdot 4H_2O$ at 4.2 K

O(1)–Cu(1)–O(2)	85.4(4)	O(1)–Cu(2)–O(2)	86.0(4)
N(1)–Cu(1)–N(2)	79.3(3)	N(3)–Cu(2)–N(4)	80.9(2)
O(1)–Cu(1)–N(1)	95.5(4)	O(1)–Cu(2)–N(3)	93.9(4)
O(2)–Cu(1)–N(2)	97.9(4)	O(2)–Cu(2)–N(4)	96.6(4)
O(7)–Cu(1)–O(1)	93.8(4)	O(3)–Cu(2)–O(1)	97.7(4)
O(7)–Cu(1)–O(2)	92.8(5)	O(3)–Cu(2)–O(2)	92.1(4)
O(7)–Cu(1)–N(1)	97.0(5)	O(3)–Cu(2)–N(3)	102.0(3)
O(7)–Cu(1)–N(2)	97.4(3)	O(3)–Cu(2)–N(4)	93.1(5)
O(1)–Cu(1)–N(2)	168.1(4)	O(1)–Cu(2)–N(4)	168.7(5)
O(2)–Cu(1)–N(1)	170.1(6)	O(2)–Cu(2)–N(3)	165.8(5)
Cu(1)–O(1)–H(1)	101.5(7)	Cu(2)–O(1)–H(1)	94.0(13)
Cu(1)–O(2)–H(2)	108.9(17)	Cu(2)–O(2)–H(2)	114.0(8)
Cu(1)–O(1)–Cu(2)	94.3(5)	Cu(2)–O(3)–S	137.7(12)
Cu(1)–O(2)–Cu(2)	93.9(5)	H(91)–O(9)–H(92)	103.8(19)
H(71)–O(7)–H(72)	109.5(28)	H(101)–O(10)–H(102)	103.2(18)
H(81)–O(8)–H(82)	100.4(21)	H(111)–O(11)–H(112)	108.7(25)

Table 6. Selected unique intramolecular and intermolecular contact distances (Å) in $[(H_2O)(bipy)Cu(OH)_2Cu(bipy)(OSO_3)]\cdot 4H_2O$ at 4.2 K. For the latter, all contacts <4 Å involving Cu atoms, and all O · · · O contacts <3.6 Å are listed *

Cu(1) · · · Cu(2)	2.896(7)	O(2) · · · O(9)	2.74(2)
Cu(1) · · · O(3)	3.89(1)	O(2) · · · O(6^{II})	2.67(1)
Cu(1) · · · O(5)	3.68(1)	O(3) · · · O(9)	3.34(1)
Cu(1) · · · O(9)	4.00(2)	O(4) · · · O(9)	2.71(1)
Cu(1) · · · O(10)	3.99(1)	O(4) · · · O(11)	3.39(2)
Cu(1) · · · O(6^{II})	3.97(1)	O(6) · · · O(11)	2.64(2)
Cu(1) · · · C(41^{III})	3.83(1)	O(7) · · · O(10)	3.47(1)
Cu(2) · · · O(5)	3.48(1)	O(7) · · · O(8^{I})	2.61(2)
Cu(2) · · · O(7)	3.68(2)	O(7) · · · O(5^{II})	2.61(1)
Cu(2) · · · O(9)	4.02(1)	O(7) · · · O(6^{II})	3.53(2)
Cu(2) · · · C(33^{IV})	3.58(1)	O(8) · · · O(9)	2.66(1)
Cu(2) · · · C(43^{IV})	3.67(1)	O(8) · · · O(11^{II})	2.80(1)
O(1) · · · O(2)	2.69(1)	O(10) · · · O(8^{I})	2.88(1)
O(1) · · · O(5)	2.81(1)	O(10) · · · O(11^{I})	2.83(1)
O(1) · · · O(10)	2.81(2)		

* Roman numeral superscripts refer to the following co-ordinate transformations: I $-1+x, y, z$; II $x, y, 1+z$; III $-x, -y, -z$; IV $x, \frac{1}{2}-y, \frac{1}{2}+z$.

determined from a difference synthesis, and the refinement of its position proceeded smoothly. Difference syntheses performed after the final refinement cycles, with and without atom H(101) included, indicated that this atom had refined to its correct position.

The environment of each copper atom in the binuclear complex is distorted square-pyramidal. The two bridging oxygen atoms and the two nitrogen atoms of one of the bipy ligands form the basal plane for each copper atom. These basal atoms are planar to a high degree; maximum deviations of atoms in the N_2O_2 planes are 0.01 Å in the case of the Cu(1) basal plane [with Cu(1) displaced 0.181 Å from the plane towards the apical water molecule], and 0.03 Å in the case of the Cu(2) basal plane [with Cu(2) displaced 0.215 Å from the plane towards the apical sulphate anion]. The dihedral angle between the two basal planes is 8.8° at 4.2 K.

Modelling the Magnetic Data.—A Fourier projection of the observed F_M data onto the *ab* crystal plane (Figure 2) reveals positive peaks of spin density centred on the two copper atom sites, and smaller peaks associated with the bridging oxygen atoms. Slight asphericity can be seen in the spin

Table 7. Hydrogen atoms bonded to oxygen atoms with a near oxygen contact (O′) in $[(H_2O)(bipy)Cu(OH)_2Cu(bipy)(OSO_3)]\cdot 4H_2O$ at 4.2 K *

Bonded atoms	O–H/Å	O′	O′ · · · H/Å	O · · · O′/Å	OHO′/°
O(1)–H(1)	1.09(2)	O(5)	1.72(2)	2.81(1)	174
O(2)–H(2)	0.97(1)	O(6^{II})	1.72(1)	2.67(1)	168
O(7)–H(71)	0.90(2)	O(5^{II})	1.72(2)	2.62(1)	177
O(7)–H(72)	0.87(3)	O(8^{I})	1.75(3)	2.61(2)	172
O(8)–H(81)	1.01(2)	O(9)	1.65(2)	2.66(1)	177
O(8)–H(82)	1.01(2)	O(11^{II})	1.79(2)	2.80(1)	178
O(9)–H(91)	0.94(1)	O(4)	1.80(1)	2.71(1)	162
O(9)–H(92)	1.20(3)	O(2)	1.55(3)	2.74(2)	170
O(10)–H(101)	1.13(3)	O(1)	1.70(3)	2.81(2)	167
O(10)–H(102)	0.90(2)	O(8^{I})	1.99(2)	2.88(1)	173
O(11)–H(111)	0.76(3)	O(6)	1.88(3)	2.64(2)	177

* Roman numeral superscripts are as in Table 6. H(112) is not involved in hydrogen bonding.

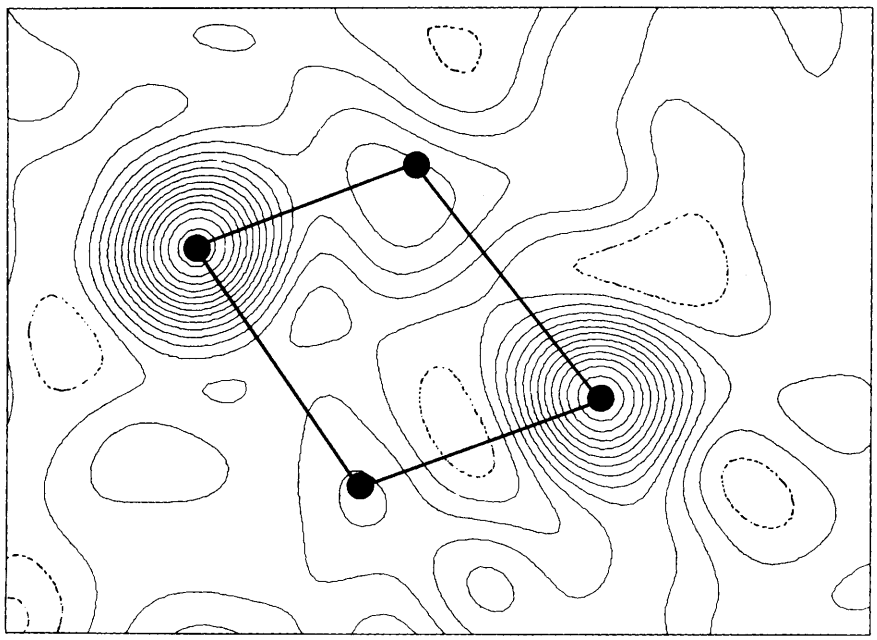

Figure 2. Fourier projection of the observed magnetic data projected on the (0 0 1) crystal plane. Broken contour lines represent negative spin density, the first continuous contour being the zero level. Contour intervals are 0.05 B.M. Å^{-3} averaged over a square of edge 0.1 Å

Table 8. Refined multipole spin populations (electrons) and agreement factors [a] for spin-density distribution models of $[(H_2O)(bipy)Cu(OH)_2Cu(bipy)(OSO_3)]\cdot 4H_2O$, based on NO = 150 magnetic data at 4.2 K. The refined κ values (a scaling parameter of the radial distribution function) for the oxygen centres were fixed from a scalar-only refinement. The populations are scaled to total two spins within the complex as no magnetisation measurements at 4.2 K are available

Centre	Variable	R1	R2	R3	R4	R5	R6 [b]
Cu(1)	Z_0^0	1.016(4)	1.024(6)	0.936(4)	0.923(5)	0.920(5)	0.847(5)
	Z_1^1	—	−0.019(4)	−0.031(3)	−0.030(3)	−0.023(4)	−0.015(3)
	Z_1^{-1}	—	−0.013(4)	−0.003(3)	−0.010(3)	−0.005(4)	−0.000(3)
	Z_2^2	—	0.067(8)	0.070(7)	0.052(7)	0.040(7)	0.048(7)
	Z_2^{-2}	—	−0.36(2)	−0.20(2)	−0.19(2)	−0.18(2)	−0.15(2)
	Z_3^3	—	0.01(1)	−0.01(1)	0.00(1)	0.01(1)	0.01(1)
	Z_3^{-3}	—	−0.03(2)	0.05(1)	0.01(2)	−0.00(2)	0.01(1)
	Z_4^4	—	−0.18(3)	−0.14(3)	−0.11(3)	−0.07(3)	−0.05(3)
	Z_4^{-4}	—	−0.01(3)	−0.10(3)	−0.01(3)	0.07(3)	0.05(3)
	κ	1.0	1.07(1)	1.07(1)	1.07	1.07	1.07
Cu(2)	Z_0^0	0.984(5)	0.976(8)	0.888(6)	0.884(6)	0.880(6)	0.810(5)
	Z_1^1	—	0.025(4)	0.006(4)	−0.009(4)	−0.006(4)	0.002(4)
	Z_1^{-1}	—	0.007(4)	−0.014(4)	−0.013(4)	−0.004(4)	−0.005(4)
	Z_2^2	—	−0.042(8)	−0.039(7)	−0.041(7)	−0.039(7)	−0.032(7)
	Z_2^{-2}	—	−0.16(2)	−0.13(2)	−0.10(2)	−0.09(2)	−0.06(2)
	Z_3^3	—	−0.05(1)	−0.05(1)	−0.06(1)	−0.02(1)	−0.02(1)
	Z_3^{-3}	—	0.04(2)	0.06(1)	0.02(1)	−0.01(1)	−0.01(1)
	Z_4^4	—	−0.07(3)	−0.05(2)	−0.03(2)	−0.10(3)	−0.08(2)
	Z_4^{-4}	—	−0.22(3)	−0.14(3)	−0.10(3)	−0.04(3)	−0.03(3)
	κ	1.0	1.10(1)	1.11(1)	1.11	1.11	1.11
O(1)	Z_0^0	—	—	0.069(4)	0.081(4)	0.088(4)	0.094(4)
	Z_1^1	—	—	—	0.027(4)	0.018(4)	0.017(4)
	Z_1^{-1}	—	—	—	−0.006(4)	−0.012(4)	−0.010(4)
	Z_2^2	—	—	—	—	0.012(7)	0.016(7)
	Z_2^{-2}	—	—	—	—	−0.033(21)	−0.037(20)
	κ	—	—	1.61(16)	1.61	1.61	1.61
O(2)	Z_0^0	—	—	0.107(4)	0.112(4)	0.112(4)	0.121(4)
	Z_1^1	—	—	—	0.034(4)	0.030(4)	0.022(4)
	Z_1^{-1}	—	—	—	0.029(4)	0.035(4)	0.031(4)
	Z_2^2	—	—	—	—	0.002(6)	0.007(6)
	Z_2^{-2}	—	—	—	—	−0.200(18)	−0.154(17)
	κ	—	—	1.14(7)	1.14	1.14	1.14
R		0.252	0.246	0.218	0.211	0.204	0.200
R'		0.196	0.170	0.130	0.120	0.111	0.106
χ		4.09	3.79	2.95	2.72	2.56	2.48
No. of variables, NV		2	20	24	24	28	32

[a] The agreement factors R, R', and χ are defined by $\Sigma|\Delta F|/\Sigma|F_o|$, $[\Sigma w(\Delta F)^2/\Sigma w F_o^2]^{\frac{1}{2}}$, and $[\Sigma w(\Delta F)^2/(NO - NV)]^{\frac{1}{2}}$ (NO = no. of observations) respectively, where $w = 1/\sigma^2(F_o)$ is the weight assigned to the F_o values, $\Delta F = F_o - F_c$, and F_o and F_c are the observed and calculated magnetic structure factors. [b] In refinement model R6, scalar Z_0^0 values were refined on the nitrogen centres N(1), N(2), N(3), and N(4) with final values 0.008(5), 0.040(6), 0.045(6), and 0.036(7) respectively for κ(N) = 1.0.

density about the copper atoms, but only a very limited qualitative interpretation of such a Fourier map is possible because of series termination errors, thermal smearing, and the effects of correlation of neighbouring points in the Fourier density. For this reason the approach used in the present analysis is that of fitting, by a least-squares procedure, structure factors calculated from a multipole spin-density model to the observed F_M data.

The unpaired electron density in the unit cell is expressed in in spherical polar co-ordinates r, θ, Φ as a superposition of one-centre density functions expanded as a linear sum of density fragments of the type [11,22] shown by equation (1), with $l = 0, 1, 2, \ldots \infty$ and $-l \leq m \leq l$, where M_l^m, N_l^m, and Z_l^m

$$\rho_{lm}(r,\theta,\varphi) = M_l^m N_l^m Z_l^m(\theta,\varphi) R_l(r)/4\pi \qquad (1)$$

are, respectively, multipole populations, normalisation factors, and Tesseral harmonics. The parameter $R_l(r)$ is the radial function for the appropriate centre, and can be varied using, for example, the ' kappa refinement ' method.[23,24] The calculated structure factor, $F_c(\mathbf{h})$, is then of the form of equation (2), where $\langle j_{j,l} \rangle$ are the Fourier Bessel transforms of the radial function $R_l(r)$ of the centre j derived [11] from the atomic orbital basis functions of Clementi and Roetti,[25] $\mathbf{h} = (h, k, l)$ are Miller indices with respect to the reciprocal lattice cell edges, and $\mathbf{x}_j$ and β_j are the positional co-ordinate and thermal tensor of centre j respectively, obtained from the nuclear structure refinement.

While it has been shown [11] that multipole populations can often be interpreted in terms of ' orbital ' populations, in cases of low crystal symmetry where orbital interpretation is difficult, an alternative interpretation of the multipole analysis is possible. We construct the density resulting from the superposition of the density fragments ρ_{lm} within a sphere containing the centres j in the region of interest. This synthesised ' at rest ' density, $\rho(\mathbf{r})$, is given by equation (3), which is calculated

$$F_c(\mathbf{h}) = \sum_{\text{cell}} \left\{ \sum_{l=0}^{\infty} \sum_{m=-l}^{l} i^l M_{j,l}^m N_l^m 4\pi \langle j_{j,l} \rangle Z_l^m(\alpha,\beta) \exp[-i2\pi \mathbf{h}\mathbf{x}_j - \mathbf{h}^T\beta_j\mathbf{h}] \right\} \qquad (2)$$

Table 9. Tesseral harmonics and normalisation constants associated with the non-vanishing multipole populations (listed in Table 8) expressed in terms of the angular components of the Bragg vector relative to the local Cartesian axes of each centre as in Figure 3. The notation is that of ref. 11

l	m	Z_l^m (α,β)	$N_l^m/4\pi$
0	0	1	0.079 577
1	1	$\sin\alpha\cos\beta$	0.318 310
1	−1	$\sin\alpha\sin\beta$	0.318 310
2	2	$3\sin^2\alpha\cos2\beta$	0.125
2	−2	$3\sin^2\alpha\sin2\beta$	0.125
3	3	$15\sin^3\alpha\cos3\beta$	0.028 294
3	−3	$15\sin^3\alpha\sin3\beta$	0.028 294
4	4	$105\sin^4\alpha\cos4\beta$	0.004 464 2
4	−4	$105\sin^4\alpha\sin4\beta$	0.004 464 2

$$\rho(\mathbf{r}) = \sum_j \sum_{lm} \rho_{lm}{}^j(r_j, \theta_j, \varphi_j) \qquad (3)$$

from the multipole populations derived from the least-squares refinement. Provided tests are carried out on the completeness of the multipole expansion, such an analysis is not subject to the distortion effects of Fourier series based on simple inversion of the magnetic structure factors. In effect, the least-squares process has been used to remove noise from the Fourier maps.

A series of multipole refinements of the F_M data are listed in Table 8. Since only two-dimensional data are available, only those multipoles spanning the two dimensions (Table 9) are used in the analysis. These functions are the scalar $Z_0{}^0$, the dipoles $Z_1{}^1$ and $Z_1{}^{-1}$, the quadrupoles $Z_2{}^2$ and $Z_2{}^{-2}$, the octapoles $Z_3{}^3$ and $Z_3{}^{-3}$, and the hexadecapoles $Z_4{}^4$ and $Z_4{}^{-4}$. Multipoles to the hexadecapole level were included for the copper atom sites. For the bridging oxygen atoms, successive refinements used increasingly higher-order multipole functions from the scalar level only (R3, Table 8), through scalar and dipole functions (R4, Table 8), to the inclusion of a scalar, dipoles, and quadrupoles (R5, Table 8). Refinement R6 (Table 8) also included scalar functions on the four nitrogen atoms co-ordinated to the copper atoms. The κ values (radial scaling parameters [23]) for the copper and oxygen atom radial functions were fixed from an initial refinement employing multipoles of only the scalar level. This was done because simultaneous refinement of the κ values with both the full copper multipole set and the bridging oxygen atom multipoles caused ill conditioning of the least-squares matrix. An independent experimental measurement of the magnetisation of $[(H_2O)(bipy)Cu(OH)_2Cu(bipy)(OSO_3)]\cdot4H_2O$ at 4.2 K and 4.6 T and with the magnetic field aligned along the c crystal axis is not available to scale the multipole populations. These have therefore been normalised to two unpaired electrons per molecule. The local Cartesian axis systems to which the multipole populations are referred are shown in Figure 3.

Plots of the spin density projected onto the *ab* plane are given in Figure 4 for four of the refinement models presented in Table 8. The spin density has been synthesised from each refinement model *via* equation (3), within a sphere of radius 4 Å from the midpoint of the Cu · · · Cu vector. Observed and calculated (refinement R6) magnetic structure factors are given in SUP No. 23495.

Interpretation of Multipole Analyses.—The general picture which emerges from a comparison of the synthesised ' at rest ' spin densities from the multipole analyses (Figure 4) is that resolution of the density on the bridging oxygen atoms is obtained on the inclusion of higher-order Tesseral harmonics.

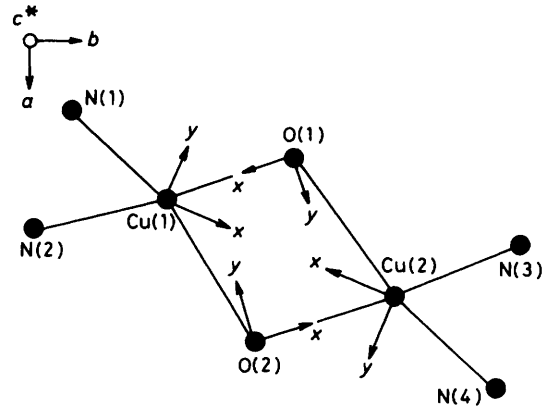

Figure 3. The local Cartesian axes to which the multipole populations are referred

There is considerable noise evident in the density about the O(1) oxygen site. However, there is general agreement in spin-density features in three of the four copper–oxygen bonds. The multipole populations can be analysed to deduce a total spin population of *ca.* 0.1 electron on each bridging oxygen atom of the hydroxy groups. Although the composition and shape of the distribution of this population varies with the level of the model used in refinement, its net magnitude does not change markedly.

The spin populations of the nitrogen donor atoms are deduced to be *ca.* 0.05 e each, quite distinctly less than for the bridging oxygen atoms. This population is presumably delocalised to some extent into the aromatic ring system of the ligands. Unfortunately, limitations in the amount and quality of the data prevent a detailed analysis, such as was undertaken for the oxygen atoms, of the composition and shape of the nitrogen atom spin distribution. Bearing in mind the behaviour of the oxygen atom spin populations with the level of refinement, it seems probable, however, that the net amount of spin found in the vicinity of the nitrogen atoms is not seriously in error.

The spin densities projected on to the copper atoms are of approximate four-fold symmetry. As expected on the grounds of the ligand site symmetries, the maxima are directed towards the ligand donor atom positions, and correspond to the half-occupancy of the $d_{x^2-y^2}$ orbital. The populations are, on average, 0.85 e, but it should be noted that these include contributions from the co-ordinated water molecule in one case, and from the co-ordinated sulphate group in the other.

The two bridging oxygen atoms show well defined and very similar regions of negative spin density directed so as to bisect the bonds to the copper atoms, but on the reverse side of the atom. The theory of magnetic exchange by the superexchange mechanism has received attention over a considerable period of time since its initial formulation.[26] However, the treatments have remained essentially qualitative in nature. It has been possible to rationalise the fact that the value of $2J$ in di-μ-hydroxo-bridged copper(II) dimers of the type of the present compound varies linearly with the Cu–O–Cu bond angle upon simple valence bond arguments,[27] on simple molecular orbital arguments,[6,7] and on a ligand-field angular overlap model.[28]

For example, it is argued that overlap of the two $3d_{x^2-y^2}$ orbitals on the copper atoms with bridging oxygen $2s$ orbitals leads to a tendency for paired spins, while overlap with a pair of oxygen $2p$ orbitals, because of internal coupling within the oxygen atom, causes the copper atom spins to align parallel. Obviously, since both the $2s$ and the $2p$ orbitals of the oxygen atom are likely to be involved in the bonding, the overall

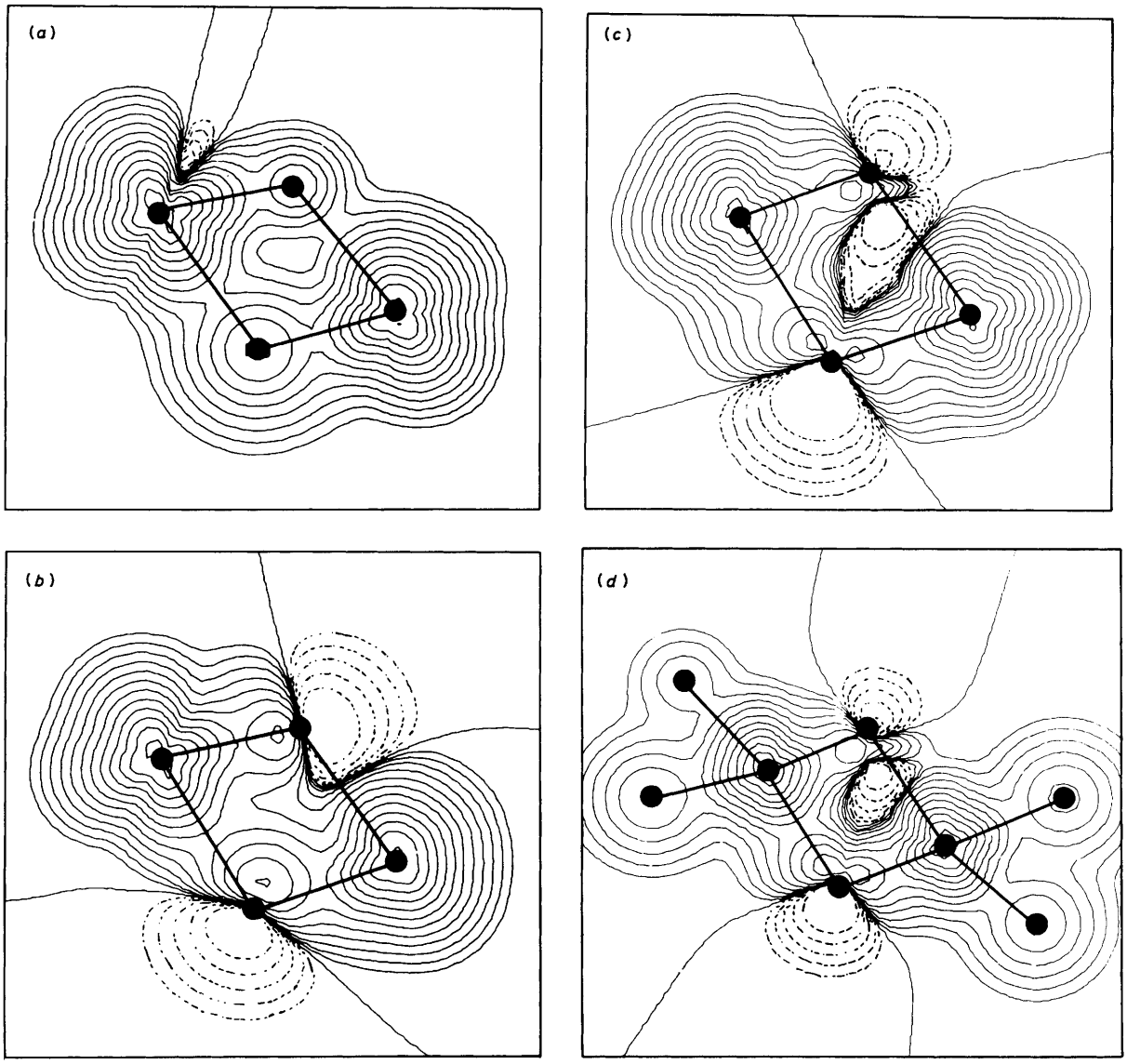

Figure 4. The spin density in $[(H_2O)(bipy)Cu(OH)_2Cu(bipy)(OSO_3)]\cdot 4H_2O$ projected on the (0 0 1) crystal plane. The plots were obtained from the multipole refinement of the magnetic data with (*a*) scalars, (*b*) scalars and dipoles, and (*c*) scalars, dipoles, and quadrupoles on the bridging oxygen atoms. In (*d*), scalar functions are also included on the four co-ordinated nitrogen atoms. The plots correspond to the multipole populations from refinements R3—6 respectively (Table 8). The broken contour lines represent negative spin density, with the first continuous contour being the zero level. Each *n*th succeeding contour represents the $2^{n-1} \times 10^{-3}$ e Å^{-3} contour level

result may be either a net antiferromagnetic copper–copper coupling (negative $2J$) if the *s* bonding effects predominate, or a net ferromagnetic coupling (positive $2J$) if the *p* orbital bonding effects are the larger. On this basis, the change from ferromagnetic coupling for Cu–O–Cu angles near 90°, when *p* overlap would maximise, to antiferromagnetic coupling at larger angles, can be rationalised. These considerations have been formalized to give a relationship between the value of $2J$ and the energies of appropriate molecular orbitals of the Cu_2O_2 system.[6,7] However, basically these treatments have lacked the information necessary to have quantitative predictive power; the sign, let alone the absolute magnitude of $2J$, could not be predicted from first principles.

In spite of the quantitative shortcomings of the treatments mentioned above, they do involve the feature that the basis of the copper–copper spin coupling is the covalent transfer of spin from the copper atoms to the bridging oxygen atoms, although they do not accurately relate $2J$ to the magnitude of that transfer. Our results demonstrate directly this superexchange mechanism for the magnetic exchange coupling between the copper atoms in the compound of study. We observe a net transfer of some 10% of the spin on to the bridging oxygen atoms. At first sight it would seem attractive for us to attempt to perform an oxygen-orbital population analysis based upon the multipole representation of the spin distribution, so that relative contributions of 2*s* and 2*p* oxygen orbitals might be assessed. However, apart from the severe limitations that would be placed on the meaning of such an analysis as discussed below, it probably would not provide information directly relevant to a quantitative treatment of the exchange phenomenon. It should be noted that the covalent transfer involves spin of the same sign; this process cannot account for the negative spin density we observe as a major feature ' behind ' the oxygen atoms.

Recently, deeper insight has been obtained into the superexchange process. Workers [29,30] have examined the process using unconstrained Hartree–Fock and $X\alpha$ calculation procedures. While a direct treatment of the Cu–O–Cu system was not involved, the results are very pertinent. A feature was the important role played by configurational interaction effects. These are manifested in the present context as spin polarisation effects. A proper account of the exchange in a di-μ-hydroxo-bridged copper dimer must be based upon a full unconstrained Hartree–Fock treatment of the Cu_2O_2 system, and that is not available at this stage. Nevertheless, our results strongly confirm the necessity for such a treatment of the problem; the negative spin density 'behind' the bridging oxygen atoms can *only* arise from spin polarisation effects, and the fact that they are such a strong feature of the spin density distributions at the oxygen atoms emphasises the role this phenomenon plays in the exchange process.

Conclusions

The need to account for spin polarisation effects in the interpretation of the redistribution of spin density which follows covalent bond formation has been shown in spin density studies of the smaller complexes $[CrF_6]^{3-}$ and $[CoCl_4]^{2-}$.[12,31,32] Spin polarisation arises because the presence of, say, positive spin tends to enhance the amount of parallel spin in its vicinity, and concomitantly to create negative (antiparallel) spin elsewhere. It occurs as a result of electron correlation effects, and so is very difficult to quantify in a system as large as a transition-metal ion. The spin densities derived in the above analysis [Figure 4(*b*)—(*d*)] are consistent with the presence of such spin polarisation effects. The present study indicates, therefore, that electron correlation must be fully included in any theoretical treatment of the exchange phenomenon.

Acknowledgements

We thank the S.R.C. and the Australian Research Grants Committee for support, and the Institut Laue-Langevin for the neutron diffraction facilities made available.

References

1 C. M. Harris, E. Sinn, W. R. Walker, and P. R. Woolliams, *Aust. J. Chem.*, 1968, **21**, 631.
2 A. T. Casey, B. F. Hoskins, and F. D. Whillans, *Chem. Commun.*, 1970, 904.
3 B. F. Hoskins and F. D. Whillans, *J. Chem. Soc., Dalton Trans.*, 1975, 1267.
4 A. T. Casey, *Aust. J. Chem.*, 1972, **25**, 2311.
5 J. A. Barnes, W. E. Hatfield, and D. J. Hodgson, *Chem. Commun.*, 1970, 1593.
6 J. A. Barnes, D. J. Hodgson, and W. E. Hatfield, *Inorg. Chem.*, 1972, **11**, 144.
7 P. J. Hay, J. C. Thibeault, and R. Hoffmann, *J. Am. Chem. Soc.*, 1975, **97**, 4884.
8 V. H. Crawford, H. W. Richardson, J. R. Wasson, D. J. Hodgson, and W. E. Hatfield, *Inorg. Chem.*, 1976, **15**, 2107.
9 B. N. Figgis, R. Mason, A. R. P. Smith, and G. A. Williams, *J. Am. Chem. Soc.*, 1979, **101**, 3673.
10 F. A. Wedgwood, *Proc. R. Soc. London, Ser. A*, 1976, **349**, 447.
11 J. N. Varghese and R. Mason, *Proc. R. Soc. London, Ser. A*, 1980, **372**, 1.
12 B. N. Figgis, P. A. Reynolds, and G. A. Williams, *J. Chem. Soc., Dalton Trans.*, 1980, 2348.
13 B. N. Figgis, P. A. Reynolds, G. A. Williams, R. Mason, A. R. P. Smith, and J. N. Varghese, *J. Chem. Soc., Dalton Trans.*, 1980, 2333.
14 B. N. Figgis, P. A. Reynolds, and G. A. Williams, *J. Chem. Soc., Dalton Trans.*, 1980, 2339.
15 G. A. Williams, B. N. Figgis, and R. Mason, *J. Chem. Soc., Dalton Trans.*, 1981, 734.
16 B. N. Figgis, G. A. Williams, J. B. Forsyth, and R. Mason, *J. Chem. Soc., Dalton Trans.*, 1981, 1837.
17 R. Mason, A. R. P. Smith, J. N. Varghese, B. N. Figgis, and G. A. Williams, *Chem. Phys. Lett.*, 1981, **79**, 366.
18 M. S. Lehmann and S. Wilson, Internal Report, Institut Laue-Langevin, Grenoble, 1979.
19 J. M. Stewart, 'The X-Ray System,' Technical Report TR 72–192, Computer Science Centre, University of Maryland, July 1972 (version of June 1973 implemented at Atlas Computer Laboratory).
20 'International Tables for *X*-Ray Crystallography,' Kynoch Press, Birmingham, 1974, vol. 4, p. 270.
21 P. J. Brown, J. B. Forsyth, and R. Mason, *Philos. Trans. R. Soc. London, Ser. B*, 1980, **290**, 481.
22 R. F. Stewart, *J. Chem. Phys.*, 1973, **58**, 1668; R. F. Stewart, *Acta Crystallogr., Sect. A*, 1976, **32**, 565.
23 P. Coppens, T. N. Guru Row, P. Leung, E. D. Stevens, P. J. Becker, and Y. W. Yang, *Acta Crystallogr., Sect. A*, 1979, **35**, 63.
24 B. N. Figgis, E. S. Kucharski, and G. A. Williams, *J. Chem. Soc., Dalton Trans.*, 1980, 1515.
25 E. Clementi and C. Roetti, *At. Data Nucl. Data Tables*, 1974, **14**, 177.
26 P. W. Anderson, *Phys. Rev.*, 1959, **115**, 2.
27 D. J. Hodgson, *Prog. Inorg. Chem.*, 1975, **19**, 173.
28 A. Bencini and D. Gatteschi, *Inorg. Chim. Acta*, 1978, **31**, 11.
29 A. P. Ginsberg, *J. Am. Chem. Soc.*, 1980, **102**, 111.
30 L. Noodleman, *J. Chem. Phys.*, 1981, **74**, 5737.
31 R. Mason, A. R. P. Smith, J. N. Varghese, G. S. Chandler, B. N. Figgis, R. A. Phillips, and G. A. Williams, *J. Am. Chem. Soc.*, 1981, **103**, 1300.
32 G. S. Chandler, B. N. Figgis, R. A. Phillips, P. A. Reynolds, R. Mason, and G. A. Williams *Proc. R. Soc. London, Ser. A*, 1982, **384**, 31.

Received 2nd *July* 1982; *Paper* 2/1112